Epitope-Specific Monoclonal Antibodies to FSHβ Increase Bone Mass

[^1,2]Yaoting Ji, [^1]Peng Liu, [^1]Tony Yuen, [3]Shozeb Haider, [4]Jiahuan He, [3]Rachel Romero, [5]Hao Chen, [1]Madison Bloch, [1]Se-Min Kim, [1]Daria Lizneva, [1]Lubna Munshi, [1]Chunxue Zhou, [1]Ping Lu, [1]Jameel Iqbal, [5]Zhen Cheng, [1]Maria New, [4]Aaron J Hsueh, *[2]Zhuan Bian, *[4]Clifford Rosen, *[1]Li Sun, *[1]Mone Zaidi

[1]The Mount Sinai Bone Program, Icahn School of Medicine at Mount Sinai, New York NY 10029, USA; [2]School and Hospital of Stomatology, Wuhan University, and Key Laboratory of Oral Biomedicine, Ministry of Education, Wuhan, Hubei 430079, China; [3]Department of Pharmaceutical and Biological Chemistry, University College London School of Pharmacy, London WC1 1AX, UK; [4]Department of Obstetrics and Gynecology, Stanford University School of Medicine, Stanford, CA 94305, USA; [5]Molecular Imaging Program at Stanford (MIPS), Bio-X Program, Department of Radiology, Stanford University, Stanford, CA 94305, USA; [6]Maine Medical Center Research Institute, Scarborough, Maine 04074, USA.

[^]Equal contribution; *joint senior authors

Correspondence: Mone Zaidi and Maria I. New

mone.zaidi@mssm.edu

maria.new@mssm.edu

Fax: 212-426-8312

ABSTRACT

Pituitary hormones have long been thought solely to regulate single targets. Challenging this paradigm, we discovered that both anterior and posterior pituitary hormones, including FSH, had other functions in physiology. We have shown that FSH regulates skeletal integrity, and, more recently, find that the inhibition of FSH reduces body fat and induces thermogenic adipose tissue. A polyclonal antibody raised against a short, receptor-binding epitope of FSHβ was found not only to rescue bone loss post-ovariectomy, but also to display marked anti-obesity and pro-beiging actions. Questioning whether a single agent could be used to treat two medical conditions of public health importance – osteoporosis and obesity – we developed two further monoclonal antibodies, Hf2 and Mf4, against computationally defined receptor-binding epitopes of FSHβ. Hf2 has already been shown to reduce body weight, fat mass and cause beiging in mice on a high-fat diet. Here, we show that Hf2, which binds mouse Fsh in immunoprecipitation assays, also increases cortical thickness and trabecular bone volume, and microstructural parameters, in sham-operated and ovariectomized mice, noted on micro-computed tomography. This effect was largely recapitulated with Mf4, which inhibited bone resorption by osteoclasts and stimulated new bone formation by osteoblasts. These effects were exerted in the absence of alterations in serum estrogen in wild type mice. We also re-confirm the existence of Fshrs in bone by documenting the specific binding of fluorescently labeled FSH, FSH-CH, *in vivo*. Our study provides the framework for the future development of an FSH-based therapeutic that could potentially target both bone and fat.

SIGNIFICANCE STATEMENT

We have addressed the question whether osteoporosis and obesity, which often occur concurrently in postmenopausal women, can be targeted by a single agent. We have shown previously that the reproductive hormone FSH, the levels of which rise after menopause, regulates both body fat and bone mass. We now show that blocking FSH action using two purposefully designed epitope-specific antibodies protects against bone loss in mice. This positions both FSH antibodies as lead molecules for clinical development towards future use in people.

/body

INTRODUCTION

FSH levels rise when procreation ceases as a consequence of ovarian failure. This period in a woman's life is associated with marked changes in body physiology (1). Bone is lost at the most rapid rate beginning two to three years prior to the cessation of menstruation (2, 3). During this time, estrogen levels are relatively unperturbed, whereas FSH levels are rising (4), and there is a tight correlation between plasma FSH levels and bone loss, independently of estrogen levels (2). This reduced bone mass is also accompanied by increases in visceral adiposity, a disruption of energy metabolism, and decreased physical activity (5, 6). These aberrations have been shown, in clinical studies, to be reversed by pharmacologic doses of estrogen (7).

Our studies have shown that FSH directly affects both bone and fat (8, 9). We and others find that these actions of FSH are mediated through a low-abundance G protein-coupled FSH receptor (FSHR) identified on osteoclasts (9), mesenchymal stem cells (10), and adipocytes (8, 11, 12), as well as in bone tissue *in vivo* (13). Unlike the ovary where FSHR-$G_{\alpha s}$ coupling is well documented, the receptor found in bone and fat tissue couples to a $G_{\alpha i}$ protein (9), the activation of which reduces cAMP levels. In bone this translates into enhanced osteoclastogenesis and reduced osteoblastogenesis *via* reductions in MAP kinase and NFκ-B signaling (9), whereas in fat tissue, the FSHR is coupled to reduced UCP1 expression (8, 12). The crystal structure of the human FSHR-FSH complex indicates that the FSHβ subunit binds to specific amino acids in the FSHR binding groove (14). By modeling the Fshr-Fsh interaction in mouse, we developed a polyclonal antibody to a 13-amino acid sequence in the binding domain of Fshβ (12, 15, 16).

Injection of this polyclonal antibody prevented ovariectomy-induced bone loss through a dual action, notably through a reduction in bone resorption and stimulation of new bone synthesis (15). In separate studies, the antibody triggered a dramatic reduction of visceral and subcutaneous fat in not only in ovariectomized mice, but also in both male and female wild type mice that were fed on a high-fat diet or on normal chow but allowed to eat *ad libitum* (12). This phenotype was associated with profound beiging of white adipose tissue (WAT), brown adipose tissue (BAT) activation, increased cellular mitochondrial density, and a thermogenic response (12). These findings, together, have presented FSH as a therapeutic target for post-menopausal bone loss and for obesity in contexts beyond and including the menopause.

Here, we present two monoclonal antibodies directed against receptor-binding sequences of human or mouse FSHβ, but which are not species-specific. Hf2 was raised against the human FSHβ epitope and Mf4 against the mouse Fshβ epitope. Computational modeling of the mouse Fshr-Fsh complex revealed that the epitope mapped to specific amino acids in the Fsh-binding pocket of the Fshr. Both antibodies showed significant osteoprotection in ovariectomized and/or sham-operated mice. Histomorphometry on Mf4-treated ovariectomized mice further showed reduced osteoclastic bone resorption, and increased bone formation rates and osteoblast numbers. Furthermore, we find that fluorescently labeled recombinant human FSH, namely, FSH-CH1055 (FSH-CH), binds to bone tissue *in vivo*, and that injecting unconjugated FSH reverses this binding. Our findings thus establish FSH as a hormonal regulator of bone (and fat), and underscore the potential utility of humanized monoclonal antibodies for the therapy of both osteoporosis and obesity.

RESULTS

We developed two anti-FSHβ monoclonal antibodies using synthetic peptides based on the Fshr-binding sequence (LVYKDPARP**NT**QK) of mouse Fshβ that was used to generate our

polyclonal antibody. The corresponding sequence for human Fshβ is LVYKDPARP**KI**QK, which represents a two amino acid difference. We fine mapped the atomic interactions between these sequences and the respective parent FSHRs. The crystal structure of human FSH in complex with the entire ectodomain of the human FSHR (PDB id 4AY9) was used as the template for comparative modeling (Fig. 1A). High sequence identity between mouse Fshr (UniProt id Q9QWV8) and human FSHR (88%) permitted for an accurate homology model to be constructed (Fig. 1B). In the human complex, residue R44 of β-chain forms an ion pair with residue E197 of the FSHR (Fig. 1A). Residue K49 forms another stable ion pair with residue E332 of the receptor. The sulphate group of the modified residue sTyr335 acts as hydrogen bond acceptor of the backbone amines of residues Y39 and V38. Furthermore, residue Y39 forms a hydrogen bond with residue H289 of the FSHR, and residue K242 is a hydrogen bond donor to the backbone of the residue A43. The modeled mouse Fshr-Fshβ complex largely has a similar binding mode to the human complex, with an additional interaction through which residue D41 makes a hydrogen bond with residue K242 of the receptor (Fig. 1B). Of note is that the N46 and T47 residues in mouse Fshβ and corresponding K46 and I47 residues in human FSHβ were found not to interact with the respective receptors (Figs. 1A and 1B).

To further confirm the expression of Fshr in bone, we injected FSH-CH, a recombinant human FSH protein conjugated to the near-infrared II (NIR-II) fluorophore CH1055, into the tail vein of Balb/c mice. NIR-II fluorescence was detected in the ovaries and the skeleton (Fig. 1C). The binding of FSH-CH to these tissues was specific, as the NIR-II signal was attenuated in the presence of a 30-fold excess of unconjugated FSH (Fig. 1C).

The structure of both human and mouse (modeled) FSHR resembles a right hand palm, with the main body as the palm and the protruding hairpin loop as the thumb (Figs. 1A and 1B). FSHβ binds in the groove generated between the palm and the thumb. Thus, we expect that the binding of the FSHR-binding sequence to an IgG (antibody) would block the entry of FSHβ

into the receptor pocket. With experimental evidence that this is indeed the case with our mouse polyclonal Fshβ antibody (12), we generated two therapeutically-directed monoclonal antibodies against the two aforementioned FSHR-binding sequences. Namely, for antibody Mf4 and Hf2, we used appropriately elongated synthetic peptides, CLVYKDPARPNTQKV and YCYTRDLVYKDPARPKIQKTCT, respectively, for immunization (GenScript).

As a prelude to the testing of Hf2 in mice, we first determined whether it recognized mouse Fshβ. Recombinant mouse Fsh was used to spike HEK293 cell lysate, which was passed through resin with immobilized polyclonal Fsh antibody that was raised against the corresponding mouse LVYKDPARPNTQK-containing Fsh motif. Immunoblotting with Hf2 revealed a ~50 kDa band in both elution and flow-through fractions that had passed through the immobilized polyclonal Fsh antibody, whereas unspiked HEK293 cell lysate did not yield an immunoreactive FSH band in any fraction (Fig. 2A). This established that mouse FSH captured specifically by a polyclonal antibody was detected by Hf2.

We have shown previously that the antibody Hf2, when administered to male mice on a high-fat diet, triggered a reduction in visceral and subcutaneous fat and caused profound beiging (12). Here, we find that Hf2 causes an increase in tibial cortical thickness (Ct.Th) and reduction in marrow area in sham-operated mice fed on normal chow (Fig. 2B). This was accompanied by a marked increase in trabecular bone mineral density (BMD), in both sham-operated and ovariectomized mice (Fig. 2C). Statistically significant or marginal increases were also noted in fractional bone volume (BV/TV), trabecular number (Tb.N), trabecular thickness (Tb.Th), and connectivity density (Conn.D), with reciprocal decrements in trabecular spacing (Tb.Sp) (Fig. 2C). These results confirm our premise that Hf2, raised against the human FSHβ epitope, could potentially be utilized for increasing bone mass in addition to its documented effect in reducing body fat (12).

Having shown that both polyclonal antibody and Hf2 increase bone mass (15), we sought to determine whether FSH inhibition consistently translated into an osteoprotective action post-ovariectomy. Towards this, we studied, in considerable detail, the effect of a second monoclonal antibody, Mf4. We first tested whether Mf4 functionally inhibited Fsh action in reducing osteoclast formation in bone marrow cell cultures. Ficoll-separated hematopoietic stem cells were incubated in serum-containing medium [mouse serum FSH concentration: 14-40 ng/mL, (17)] with RANKL for 5 days with or without added FSH (30 ng/mL) and increasing antibody concentrations. As serum-containing medium was used, we anticipated that Mf4, by blocking the action of endogenous Fsh, would reduce osteoclastogenesis in the absence of added Fsh in a concentration-dependent manner, which was indeed the case (Fig. 3A). However, to establish FSH specificity, we spiked the medium with 30 ng/mL Fsh, and found that the stimulation by Fsh of osteoclastogenesis (seen at zero-dose of Mf4) was progressively attenuated with increasing Mf4 concentrations. This result was identical to that with the polyclonal antibody (Fig. 3B). Similarly, Hf2 inhibited osteoclastogenesis in a dose-dependent manner (Fig. 3C). The IC_{50}s of the three antibodies were in the nanomolar range (shown in Figs 3A-3C). These findings together establish that the effect of Mf4 and Hf2 in blocking osteoclast formation is mediated by blocking Fsh action.

We therefore next examined the effect of Mf4 on bone in ovariectomized and sham-operated mice. Injection of Mf4 for a short, 4-week period resulted in statistically significant or marginal increases in BMD, BV/TV, Tb.N, and Conn.D in ovariectomized and/or sham-operated mice (Fig. 3D). Histomorphometry revealed significant reductions in osteoclast number (N.Oc) and resorbed surface (Oc.S) in Mf4-treated ovariectomized mice, measured both at the spine and tibial head, indicating a potent effect of Mf4 in reducing osteoclastic bone resorption (Fig. 4A). Specifically, in the tibial head, there was a significant increase in Oc.S and N.Oc expectedly following ovariectomy, and this was reduced to baseline in Mf4-treated mice.

Consistent with the histomorphometry data, expression of osteoclast-specific genes, namely acid phosphatase 5, tartrate resistant (*Acp5,* also known as *Trap*) and matrix metalloproteinase-9 (*Mmp9*), were reduced in osteoclasts derived from Mf4-treated ovariectomized mice compared to IgG-treated control (Fig. 4B). We next studied the effect of Mf4 on bone formation by dynamic histomorphometry following dual calcein and xylelol orange labeling. Little change was noted with Mf4 treatment in the sham-operated group. However, in ovariectomized mice, Mf4 triggered significant increases in mineralized surface (MS) and bone formation rate (BFR), as well as in osteoblast numbers (Ob.N) (Figs. 4C and 4D). Importantly, Mf4 did not alter estrogen levels in wild type mice (Fig. 4D). Together, the effects of Mf4 in increasing bone mass, inhibiting bone resorption, and stimulating new bone formation were consistent with our earlier results with the polyclonal Fsh antibody raised to the same epitope (15).

DISCUSSION

Several levels of association have emerged between the two global epidemics osteoporosis and obesity, which affect 100 and 600 million people, respectively, worldwide. First, in contrast to prior assumptions that fat mass begets bone mass, it is now clear from epidemiological studies that obesity tracks with osteoporosis (18-20). Notably, there is a negative correlation between bone mass and fat mass in both rodents and in people [e.g. (18, 20)]. Second, during the menopausal transition, the rapid bone loss that leads to high fracture rates accompanies the onset of visceral fat accumulation (2, 3, 6); the latter, if left unchecked, predisposes to metabolic syndrome, cardiovascular disease, and cancer. The late perimenopause, in particular, is associated with rising FSH levels in the face of normal estrogen (4), raising the question whether estrogen deficiency is the sole cause of these physiologic aberrations. Third, bone marrow adiposity, often seen as a function of aging and sex steroid deficiency, is linked with osteoporosis (21, 22). These associations lay the basis not only for

overlapping molecular mechanisms that underpin both osteoporosis and obesity, but also for a new therapeutic approach to treat these two diseases simultaneously. We surmise that FSH, a fertility hormone, is one such molecule that regulates both osteoblast progenitors and adipocytes. This fundamental premise also makes biological sense as osteoblasts, cells that build new bone, and adipocytes derive from the same mesenchymal progenitor (23).

With a therapeutic goal in mind, rather than generating antibodies to the intact FSHβ molecule, we chose to target a short epitope that, upon computational modeling, was found to interact with specified amino acids in the ligand-binding pocket of the Fshr. We made the assumption that the binding of an IgG to that site would block entry of active FSHβ into this restricted pocket, and hence, block FSH action. Experimentally, our polyclonal and monoclonal antibodies both blocked the stimulation of osteoclastogenesis induced by specifically FSH. This finding was consistent with previous results in which the polyclonal antibody inhibited FSH-induced Ucp1 activation in dedifferentiated brown adipocytes (Thermo cells) (12).

Our proof-of-principle *in vivo* studies show that the inhibition of FSH action, either through genetic ablation of the *Fshr* or *via* pharmacological blockade using the epitope-specific FSH antibodies, results in significant osteoprotection in ovariectomized mice, and triggers the loss of body fat in multiple mouse models of obesity, including mice on a high-fat diet, mice allowed to eat *ad libitum*, and in ovariectomized mice (12, 15). Of note is that the FSH antibodies, at the dosages used, do not affect serum estrogen levels (12, 15), but this does not rule out equally relevant effects of estrogen on both bone mass and body fat (7, 24-26).

In addition to its action on bone and fat cells, we found previously that FSH directly up-regulates the production of the inflammatory cytokine TNFα (27). Mice genetically deficient in FSHβ thus showed reduced TNFα production from bone marrow macrophages (27). Furthermore, post-menopausal women, who lose bone and gain fat and have high circulating

FSH, also display elevated TNFα levels (28). Together, these findings suggest that part of the effects of FSH on bone may be TNFα-mediated. It is also possible that FSH promotes inflammation in visceral fat through TNFα production. There is mounting evidence that systemic inflammation, particularly in perivascular fat, contributes to obesity-associated cardiovascular risk (29, 30). A question arises, therefore, whether, in addition to reducing bone loss, FSH blockade might also reduce TNFα-mediated inflammation, and whether this can translate into reduced vasculopathy and cardiovascular disease.

In summary, we confirm through genetic and pharmacological strategies that blocking FSH action on its receptor promotes health by stimulating new bone formation, reducing bone removal, and inhibiting fat accumulation. One would ask whether FSH, while being critical for procreation, becomes a catabolic hormone after procreation ceases in women. And, more importantly, whether the effects of FSH, together, could contribute to alterations in longevity? Indeed, there is evidence that *Prop1*^{df} mice (Ames dwarfs) and *Ghr*$^{-/-}$ mice (Laron dwarfs) with low circulating FSH levels live longer depending on diet, gender and genetic background (31-33). This increase in longevity is associated with the maintenance of youthful levels of cognitive and neuromuscular function, and a reduced rate of aging (33). If the noted pro-aging actions are FSH-dependent, they could represent a new mechanism for the trade-off between fertility and longevity (33). Could FSH thus also be a primary aging hormone?

METHODS

For comparative modeling, we used the crystal structure of the human FSH in complex with the entire ectodomain of the human FSHR as the template (PDB id 4AY9) (14). Sequence of mouse Fshr was obtained from UniProt (id Q9QWV8) and homology construction was achieved using Modeller (34), with stereochemical parameters being checked using PROCHECK (35) and PROSA (36). For molecular dynamics (MD), 5 ns of constant number, volume and energy (NVE) MD production was carried out using a 1 fs time step; periodic boundary conditions were used; and the accuracy of the particle mesh Ewald (PME) was increased by reducing the direct sum tolerance (DSUM_TOL) by an order of magnitude (0.000001). Strong restraints were applied over the backbone atoms of the four residues surrounding the missing loop: K294-S295 and S331-D332.

To image Fshrs *in vivo*, anesthetized adult female Balb/c mice (Charles River Laboratories) were placed on a stage with a venous catheter for tail vein injection of recombinant human FSH (Sigma) that was conjugated to the near-infrared II (NIR-II) fluorophore CH1055 (13). NIR-II images were acquired using a 320×256 pixel two-dimensional indium gallium arsenide (InGaAs) photodiode array (Princeton Instruments). Stanford University Animal Ethics Committee approved the experimental protocol.

Female mice were ovariectomized, injected and sacrificed *per* protocol approved by Icahn School of Medicine at Mount Sinai's Institutional Animal Care and Use Committee. For micro-CT measurements, the L3 vertebra was scanned non-destructively by using a Scanco μCT scanner (μCT-40; Scanco Medical AG, Bassersdorf, Switzerland) at 12 μm isotropic voxel size, with X-ray source power of 55 kV and 145 μA, and integration time of 300 milliseconds (courtesy Dr. Jay Cao, USDA). The trabecular microstructure of the entire secondary spongiosa of L3 between the cranial and the caudal area was evaluated. Noise was removed from the

scanned grey-scale images using a low-pass Gaussian filter, and a fixed bone mineral density (BMD) threshold of 220 mg/cm^3 was used to extract the mineralized bone from soft tissue and the marrow phase. The reconstruction and 3D quantitative analyses were performed using software provided by Scanco. The same settings for scan and analysis were used for all samples. Trabecular bone parameters included volumetric BMD, bone volume (BV), fractional bone volume (BV/TV), trabecular thickness (Tb.Th), trabecular number (Tb.N), and trabecular spacing (Tb.Sp).

Bone formation and resorption rates were quantified by histomorphometry following two sequential injections of calcein (15 mg/kg) followed by xylelol orange (90 mg/kg) five days apart before sacrifice. Parameters included mineralized surface (MS), mineral apposition rate (MAR), bone formation rate (BFR), osteoblast number (N.Ob/BV), resorbed surface (Oc.S/BS) and osteoclast number (N.Oc/BS or N.Oc/BV). Estrogen levels were measured by ELISA (BioTang, Cat# M7619). Bone marrow was isolated from femurs and stromal cell cultures performed for 10 or 21 days according to our published protocol (37). Quantitative PCR for *Acp5* and *Mmp9* was performed using a protocol described previously (12).

ACKNOWLEDGEMENTS

M.Z. gratefully acknowledges the National Institutes of Health (NIH) for grants R01 DK80459 and DK113627 (to M.Z. and L.S.), R01 AG40132, R01 AG23176, R01 AR06592 and R01 AR06066 (to M.Z.). A grant (# 81120108010) from National Science Foundation of China, Ministry of China (International Collaborative Grant to Z.B. and M.Z.) is also gratefully acknowledged. The authors also acknowledge Mount Sinai Innovation Partners (MSIP) for their collaboration. C.J.R acknowledges support from NIH/NIGMS (P30 GM106391; P30 GM103392); NIH/NIDDK (R24 DK092759-06); Physiology Core Facility grant (P20 GM103465); and COBRE in Stem Cell Biology and Regenerative Medicine (a grant supported by NIGMS). The valuable micro-CT support from Dr. Jay Cao is also gratefully acknowledged.

DISCLOSURES

M.Z. is a named inventor on patents related to FSH and bone and FSH and fat, owned by Icahn School of Medicine at Mount Sinai. M.Z. will receive royalties and/or licensing fees *per* Mount Sinai policies, in case the patent is commercialized. M.Z. also consults for Merck, Roche, Novartis, and a number of financial consulting platforms.

REFERENCES

1. Greendale GA & Sowers M (1997) The menopause transition. *Endocrinol Metab Clin North Am* 26(2):261-277.
2. Sowers MR*, et al.* (2003) Endogenous hormones and bone turnover markers in pre- and perimenopausal women: SWAN. *Osteoporos Int* 14(3):191-197.
3. Sowers MR*, et al.* (2013) Changes in bone resorption across the menopause transition: effects of reproductive hormones, body size, and ethnicity. *J Clin Endocrinol Metab* 98(7):2854-2863.
4. Randolph JF, Jr.*, et al.* (2006) The value of follicle-stimulating hormone concentration and clinical findings as markers of the late menopausal transition. *J Clin Endocrinol Metab* 91(8):3034-3040.
5. Sowers M, Pope S, Welch G, Sternfeld B, & Albrecht G (2001) The association of menopause and physical functioning in women at midlife. *J Am Geriatr Soc* 49(11):1485-1492.
6. Thurston RC*, et al.* (2009) Gains in body fat and vasomotor symptom reporting over the menopausal transition: the study of women's health across the nation. *Am J Epidemiol* 170(6):766-774.
7. Van Pelt RE, Gavin KM, & Kohrt WM (2015) Regulation of Body Composition and Bioenergetics by Estrogens. *Endocrinol Metab Clin North Am* 44(3):663-676.
8. Liu XM*, et al.* (2015) FSH regulates fat accumulation and redistribution in aging through the Galphai/Ca(2+)/CREB pathway. *Aging Cell* 14(3):409-420.
9. Sun L*, et al.* (2006) FSH directly regulates bone mass. *Cell* 125(2):247-260.
10. Blair HC*, et al.* (2011) Skeletal receptors for steroid-family regulating glycoprotein hormones: A multilevel, integrated physiological control system. *Ann N Y Acad Sci* 1240:26-31.

11. Cui H*, et al.* (2012) FSH stimulates lipid biosynthesis in chicken adipose tissue by upregulating the expression of its receptor FSHR. *J Lipid Res* 53(5):909-917.

12. Liu P*, et al.* (2017) Blocking FSH induces thermogenic adipose tissue and reduces body fat. *Nature* 546(7656):107-112.

13. Feng Y*, et al.* (2017) Live imaging of follicle stimulating hormone receptors in gonads and bones using near infrared II fluorophore. *Chem Sci* 8(5):3703-3711.

14. Jiang X*, et al.* (2012) Structure of follicle-stimulating hormone in complex with the entire ectodomain of its receptor. *Proc Natl Acad Sci U S A* 109(31):12491-12496.

15. Zhu LL*, et al.* (2012) Blocking antibody to the beta-subunit of FSH prevents bone loss by inhibiting bone resorption and stimulating bone synthesis. *Proc Natl Acad Sci U S A* 109(36):14574-14579.

16. Zhu LL*, et al.* (2012) Blocking FSH action attenuates osteoclastogenesis. *Biochem Biophys Res Commun* 422(1):54-58.

17. Jimenez M*, et al.* (2005) Validation of an ultrasensitive and specific immunofluorometric assay for mouse follicle-stimulating hormone. *Biol Reprod* 72(1):78-85.

18. Fu X*, et al.* (2011) Associations of fat mass and fat distribution with bone mineral density in pre- and postmenopausal Chinese women. *Osteoporos Int* 22(1):113-119.

19. Zaidi M, Buettner C, Sun L, & Iqbal J (2012) Minireview: The link between fat and bone: does mass beget mass? *Endocrinology* 153(5):2070-2075.

20. Zhao LJ*, et al.* (2007) Relationship of obesity with osteoporosis. *J Clin Endocrinol Metab* 92(5):1640-1646.

21. Devlin MJ & Rosen CJ (2015) The bone-fat interface: basic and clinical implications of marrow adiposity. *Lancet Diabetes Endocrinol* 3(2):141-147.

22. Schwartz AV*, et al.* (2013) Vertebral bone marrow fat associated with lower trabecular BMD and prevalent vertebral fracture in older adults. *J Clin Endocrinol Metab* 98(6):2294-2300.

23. Zaidi M (2007) Skeletal remodeling in health and disease. *Nat Med* 13(7):791-801.

24. Kohrt WM & Wierman ME (2017) Preventing Fat Gain by Blocking Follicle-Stimulating Hormone. *N Engl J Med* 377(3):293-295.

25. Seibel MJ, Dunstan CR, Zhou H, Allan CM, & Handelsman DJ (2006) Sex steroids, not FSH, influence bone mass. *Cell* 127(6):1079; author reply 1080-1071.

26. Zaidi M, Sun L, Kumar TR, Sairam MR, & Blair HC (2006) Response: Both FSH and Sex Steroids Influence Bone Mass. *Cell* 127(6):1080-1081.

27. Iqbal J, Sun L, Kumar TR, Blair HC, & Zaidi M (2006) Follicle-stimulating hormone stimulates TNF production from immune cells to enhance osteoblast and osteoclast formation. *Proc Natl Acad Sci U S A* 103(40):14925-14930.

28. Pacifici R (1993) Cytokine production and surface antigen expression by peripheral blood mononuclear cells in postmenopausal osteoporosis. *J Bone Miner Res* 8(6):775-778.

29. Mathieu P, Lemieux I, & Despres JP (2010) Obesity, inflammation, and cardiovascular risk. *Clin Pharmacol Ther* 87(4):407-416.

30. Mathieu P, Poirier P, Pibarot P, Lemieux I, & Despres JP (2009) Visceral obesity: the link among inflammation, hypertension, and cardiovascular disease. *Hypertension* 53(4):577-584.

31. Coschigano KT*, et al.* (2003) Deletion, but not antagonism, of the mouse growth hormone receptor results in severely decreased body weights, insulin, and insulin-like growth factor I levels and increased life span. *Endocrinology* 144(9):3799-3810.

32. Westbrook R, Bonkowski MS, Strader AD, & Bartke A (2009) Alterations in oxygen consumption, respiratory quotient, and heat production in long-lived GHRKO and Ames dwarf mice, and short-lived bGH transgenic mice. *J Gerontol A Biol Sci Med Sci* 64(4):443-451.

33. Bartke A, Sun LY, & Longo V (2013) Somatotropic signaling: trade-offs between growth, reproductive development, and longevity. *Physiol Rev* 93(2):571-598.

34. Fiser A & Sali A (2003) Modeller: generation and refinement of homology-based protein structure models. *Methods Enzymol* 374:461-491.

35. Laskowski RA, MacArthur MW, Moss DS, & Thornton JM (1993) PROCHECK: a program to check the stereochemical quality of protein structures. *J Appl Cryst* 26(2):283-291.

36. Wiederstein M & Sippl MJ (2007) ProSA-web: interactive web service for the recognition of errors in three-dimensional structures of proteins. *Nucleic Acids Res* 35(Web Server issue):W407-410.

37. Liu P*, et al.* (2016) Anabolic actions of Notch on mature bone. *Proc Natl Acad Sci U S A* 113(15):E2152-2161.

38. Abagyan R, Totrov M, & Kuznetsov D (1994) ICM—A new method for protein modeling and design: Applications to docking and structure prediction from the distorted native conformation. *J Comput Chem* 15(5):488-506.

FIGURE LEGENDS

Figure 1: Interaction between the Binding Domain of Human and Mouse FSHβ and the FSH Receptor (FSHR). (**A**) The crystal structure of FSHβ in complex with the entire ectodomain of FSHR (FSHα omitted for clarity) was used as the template (PDB id 4AY9) for comparative modeling. Right panel: Dashed lines show interactions between specific amino acids of the human FSH-FSHR complex (discussed in the Results section). Of note is that K46 and I47 are non-interacting residues. (**B**) High sequence identity between mouse FSHR (uniprot id Q9QWV8) and human FSHR (88%) permitted accurate homology modeling (Modeller, PROCHECK and PROSA). The FSHβ binding epitope differs by only two amino acids (LVYKDPARP**KI**QK→LVYKDPARP**NT**QK). Several models of the mouse Fshβ epitope were constructed (ICM software) (38); restrained minimization was used to remove steric clashes; and the final model was selected on basis of the lowest Cα RMSD after superimposition on template structure (0.2 Å). Fshβ binds in the groove generated between the palm and the thumb of the Fshr. The electrostatic surfaces generate a complementary surface charge (red: acidic residues; blue: basic residues) between the Fshr and Fshβ. Since the crystal structure provides a static snapshot, a short burst of molecular dynamics (MD) simulation was run to allow the side chains of Fshr and Fshβ to dynamically equilibrate and adapt to the contours of the complex (see Methods). Right panel: Dashed lines show interactions between specific amino acids of the FSH-FSHR complex. N46 and T47 are non-interacting residues. (**C**) NIR-II imaging of Fshr-expressing ovaries and bones using FSH-CH in adult female mice. FSH-CH (12.5 μg) was injected into the tail vein of mice before *in vivo* imaging 2 h later. Left panels: Supine view showing fluorescent signals in ovaries (top), which were blocked with 30-fold excess of unconjugated FSH (bottom); this indicated hormonal specificity of signals. Middle panels: NIR-II fluorescence was detected in dissected ovaries and hind limbs (top). 30-fold

excess of unconjugated FSH blocked these signals (bottom). Right panel: Normalized florescence intensity for each tissue is shown.

Figure 2: Monoclonal Anti-Epitope FSHβ Antibody Hf2 Binds Mouse Fsh to Increase Bone Mass in Ovariectomized and Sham-Operated Mice. (**A**) Recombinant mouse Fsh (Fshα-Fshβ chimera, 2 µg) was added to lysates of HEK293 cells. Spiked and unspiked lysates were passed through resin (Pierce Co-Immunoprecipitation Kit, 26149, Thermo Scientific) with immobilized polyclonal Fsh antibody. Elution (Eluate), flow-through (Flow), and consecutive wash fractions (Wash) were collected and immunoblotted, as shown, with the monoclonal Fsh antibody Hf2. An immunoreactive band at the expected size, ~50 kD, in both elution and flow through fractions is seen in the spiked, but not in unspiked lysate. Lanes 1 and 2 were loaded with mouse FSH and lysate alone, respectively. (**B, C**) Mice were ovariectomized or sham-operated and injected with Hf2 (raised against YCYTRDLVYKDPARP**KI**QKTCT) or mouse IgG (200 µg/day) for 4 weeks while on normal chow (n=5-6 mice *per* group). The vertebral column, and in cases, the long bones were dissected and processed for micro-computed tomographic (micro-CT) measurements. Cortical bone parameters, namely cortical thickness (Ct.Th) and marrow area (Me.Ar), obtained on the mid-diaphysis of the tibia are shown (B). Representative micro-CT images and structural parameters of vertebral column (spine), namely bone mineral density (BMD), fractional bone volume (BV/TV), trabecular thickness (Tb.Th), trabecular number (Tb.N), trabecular spacing (Tb.Sp), and/or connectivity density (Conn.D), are shown (C). Statistics: Mean±SEM; Two-tailed Student's t-test, corrected for multiple comparisons; *p≤0.05, **p≤0.01, or as indicated.

Figure 3: Monoclonal Anti-Epitope FSHβ Antibody Increases Bone Mass in Ovariectomized Mice. (**A-C**) To confirm FSH specificity of the monoclonal antibodies Mf4 and

Hf2, Ficoll-purified hematopoietic stem cells were cultured with RANKL (30 ng/mL) and incubated with varying concentrations of the polyclonal FSH antibody (A), Mf4 (raised against CLVYKDPARP**NT**QKV) (B) or Hf2 (C) for 5 days in the presence or absence of mouse Fsh (30 ng/mL) (n=8 wells/group). Cells stained using a kit for tartrate-resistant acid phosphatase (Acp5) were counted. Representative culture wells are shown, together with mean percent osteoclast number (±SEM). Note that the increase in osteoclastogenesis noted with 30 ng/mL FSH (and zero-dose antibody) was abolished progressively with increasing antibody concentrations. IC_{50}s for the polyclonal FSH antibody, Mf4 and Hf2 are shown. (**D**) Mice were ovariectomized or sham-operated and injected with Mf4 or mouse IgG (100 µg/day) for 4 weeks while on normal chow (n=5 mice/group). The vertebral column was dissected and processed for micro-computed tomographic (micro-CT) measurements. Representative micro-CT images and structural parameters, namely bone mineral density (BMD), fractional bone volume (BV/TV), trabecular thickness (Tb.Th), trabecular number (Tb.N), trabecular spacing (Tb.Sp), and/or connectivity density (Conn.D), are shown. Statistics: Mean ± SEM; fwo-tailed Student's t-test, corrected for multiple comparisons; *p≤0.05, **p≤0.01, or as shown.

Figure 4: Monoclonal Anti-Epitope FSHβ Antibody Mf4 Reduces Bone Resorption and Stimulates Osteoblastic Bone Formation. The vertebral column (spine) and tibia from the mice above (Fig. 3C) were dissected and processed for Acp5 staining. Shown are representative images of Acp5-stained sections from vertebral column (spine) and tibial head (tibia), with parameters of resorption, namely osteoclast surface/bone surface (Oc.S/BS), osteoclast number/BS (N.Oc/BS) and N.Oc/bone volume (N.Oc/BV) (**A**). mRNA expression (qPCR) for *Acp5* and *Mmp9* in marrow-derived osteoclasts obtained from these mice showed reduced osteoclastogenesis in the Mf4-treated group (**B**). These mice were also injected with calcein and xylelol orange 5 days apart before sacrifice, and bones were processed for dynamic histomorphometry and alkaline phosphatase staining of osteoblasts. Shown are fluorescent

micrographs of vertebral column displaying xylelol orange (red) and calcein (green) labels, and estimates of mineralizing surface (MS), mineral apposition rate (MAR, or interlabel distance), and bone formation rate (BFR) (**C**). Alkaline phosphatase-labeled sections and calculated osteoblast number/bone volume (N.Ob/BV) are shown (**D**). Statistics: n=5 mice/group; for panel B, n=3, technical replicates; mean ± SEM; two-tailed Student's t-test, corrected for multiple comparisons; *p≤0.05, **p≤0.01, or as shown.

Fig 1

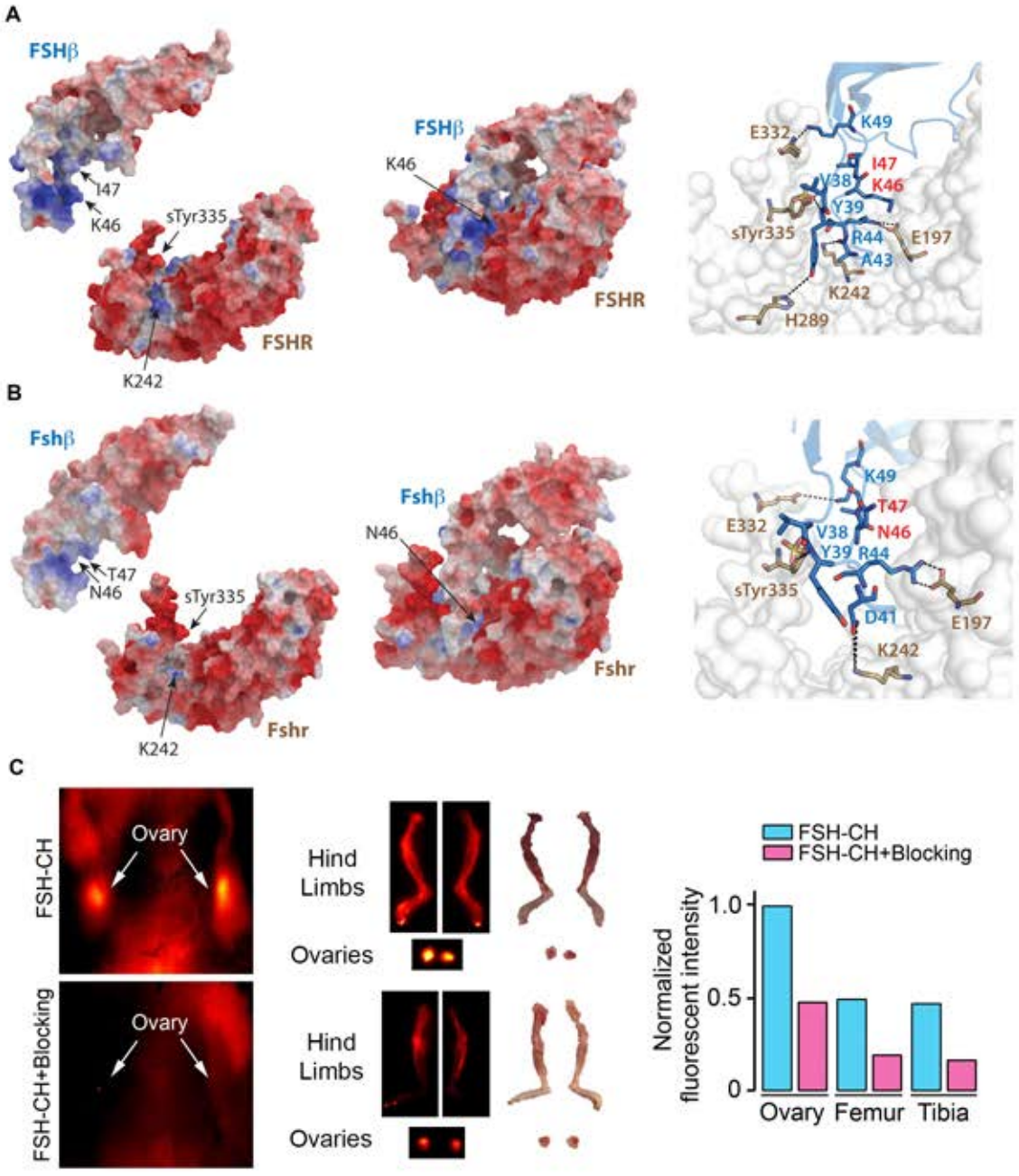
A
FSHβ
I47
K46
sTyr335
FSHR
K242
FSHβ
K46
FSHR
E332
K49
I47
K46
V38
Y39
sTyr335
R44
E197
A43
K242
H289
B
Fshβ
T47
N46
sTyr335
Fshr
K242
Fshβ
N46
Fshr
K49
T47
E332
N46
V38
Y39
R44
sTyr335
D41
E197
K242
C
FSH-CH
Ovary
FSH-CH+Blocking
Ovary
Hind Limbs
Ovaries
Hind Limbs
Ovaries
FSH-CH
FSH-CH+Blocking
Normalized fluorescent intensity
1.0
0.5
0
Ovary
Femur
Tibia

Figure 2

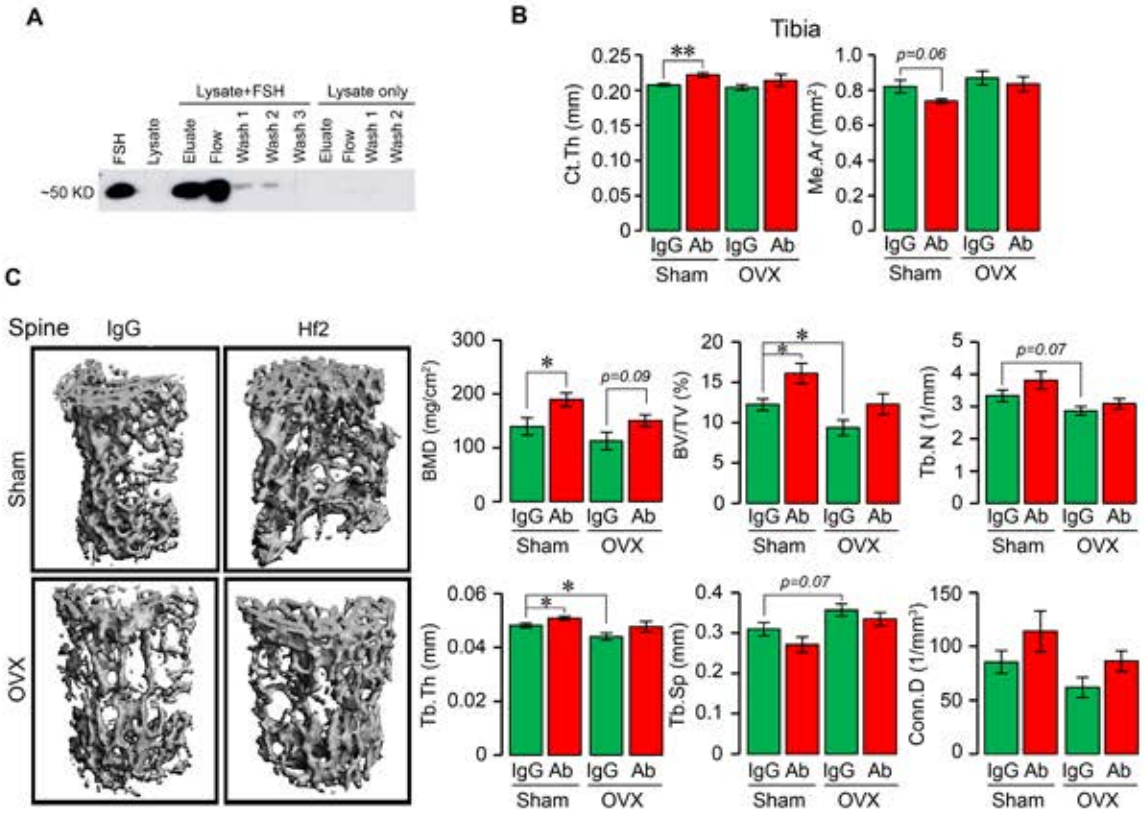
A
Lysate+FSH
Lysate only
FSH
Lysate
Eluate
Flow
Wash 1
Wash 2
Wash 3
Eluate
Flow
Wash 1
Wash 2
~50 KD
B
Tibia
Ct.Th (mm)
Me.Ar (mm²)
**
p=0.06
IgG Ab IgG Ab
Sham OVX
C
Spine
IgG
Hf2
Sham
OVX
BMD (mg/cm³)
BV/TV (%)
Tb.N (1/mm)
Tb.Th (mm)
Tb.Sp (mm)
Conn.D (1/mm³)
p=0.09
p=0.07

Figure 3

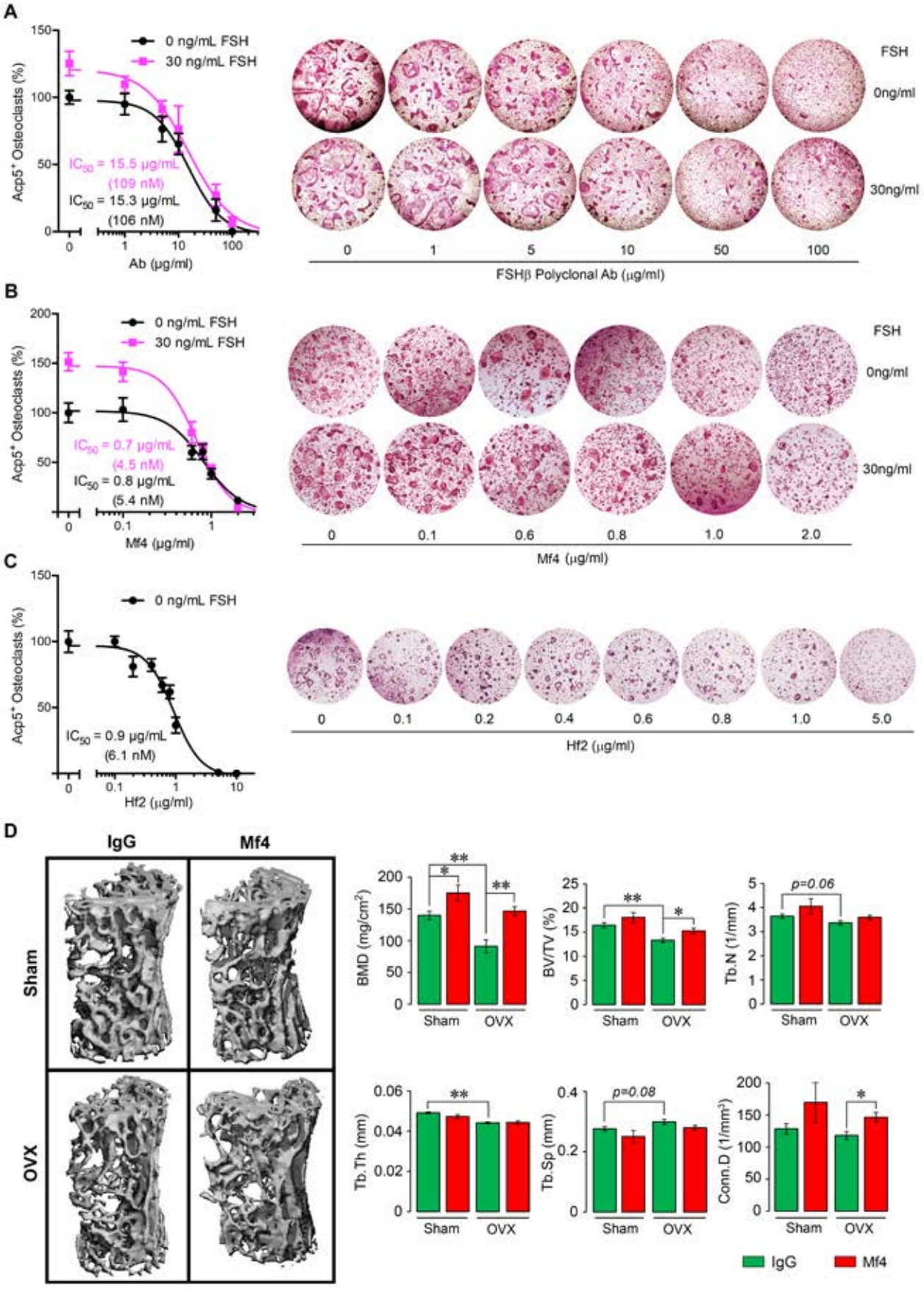
A
0 ng/mL FSH
30 ng/mL FSH
Acp5+ Osteoclasts (%)
IC50 = 15.5 μg/mL
(109 nM)
IC50 = 15.3 μg/mL
(106 nM)
Ab (μg/ml)
FSH
0ng/ml
30ng/ml
0
1
5
10
50
100
FSHβ Polyclonal Ab (μg/ml)
B
0 ng/mL FSH
30 ng/mL FSH
Acp5+ Osteoclasts (%)
IC50 = 0.7 μg/mL
(4.5 nM)
IC50 = 0.8 μg/mL
(5.4 nM)
Mf4 (μg/ml)
FSH
0ng/ml
30ng/ml
0
0.1
0.6
0.8
1.0
2.0
Mf4 (μg/ml)
C
0 ng/mL FSH
Acp5+ Osteoclasts (%)
IC50 = 0.9 μg/mL
(6.1 nM)
Hf2 (μg/ml)
0
0.1
0.2
0.4
0.6
0.8
1.0
5.0
Hf2 (μg/ml)
D
IgG
Mf4
Sham
OVX
BMD (mg/cm2)
BV/TV (%)
Tb.N (1/mm)
p=0.06
Tb.Th (mm)
Tb.Sp (mm)
p=0.08
Conn.D (1/mm3)
Sham
OVX
IgG
Mf4

Figure 4

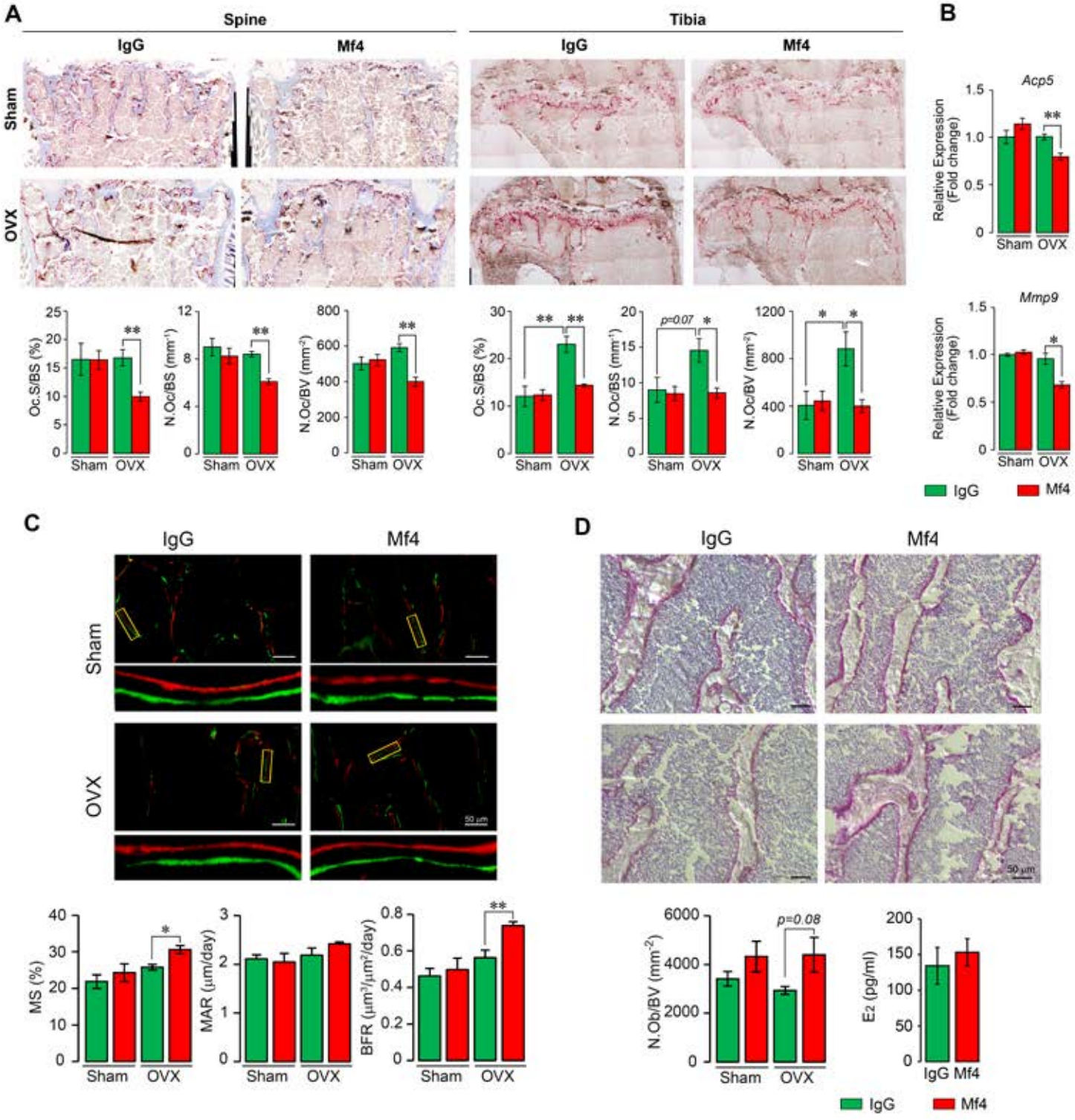
A
Spine
Tibia
IgG
Mf4
Sham
OVX
Oc.S/BS (%)
N.Oc/BS (mm⁻¹)
N.Oc/BV (mm⁻²)
p=0.07
B
Acp5
Mmp9
Relative Expression (Fold change)
C
MS (%)
MAR (μm/day)
BFR (μm³/μm²/day)
D
N.Ob/BV (mm⁻²)
p=0.08
E2 (pg/ml)